beverages

Article

Fast and Non-Invasive Evaluation of Yeast Viability in Fermentation Processes Using Raman Spectroscopy and Machine Learning

Raoul Heese [1,*,†], Jens Wetschky [2,†], Carina Rohmer [2], Susanne M. Bailer [2,3] and Michael Bortz [1]

[1] Fraunhofer Institute for Industrial Mathematics ITWM, Fraunhofer-Platz 1, 67663 Kaiserslautern, Germany; michael.bortz@itwm.fraunhofer.de

[2] Fraunhofer Institute for Interfacial Engineering and Biotechnology IGB, Nobelstraße 12, 70569 Stuttgart, Germany; jens.wetschky@igb.fraunhofer.de (J.W.); carina.rohmer@igb.fraunhofer.de (C.R.); susanne.bailer@igb.fraunhofer.de (S.M.B.)

[3] Institute for Interfacial Engineering and Plasma Technology IGVP, University of Stuttgart, Pfaffenwaldring 31, 70569 Stuttgart, Germany

* Correspondence: raoul.heese@itwm.fraunhofer.de

† These authors contributed equally to this work.

Abstract: Fermentation processes used for producing alcoholic beverages such as beer, wine, and cider have a long history, having been developed early on across different civilizations. In most instances, yeast strains are used for fermentation processes, e.g., at breweries and wineries. Monitoring of yeast viability, cell count, and growth behavior is essential to ensure a controlled fermentation process. However, classical microbiological techniques to monitor fermentation process parameters are time-consuming and require sampling, along with the risk of contamination. Nowadays, industries are moving toward automation and digitalization. This necessitates state-of-the-art process analytical technologies to ensure an efficient and controlled process to obtain high-quality product outputs. Hence, there is a strong need for a fast, non-invasive, and generally applicable method to evaluate the viability of yeast cells during fermentation to warrant the standardization and purity of produced products in industrial applications. The aim of our study is to discriminate between viable and non-viable yeast in various culture media using Raman spectroscopy (RS) followed by data analysis with machine learning (ML) tools. These techniques allow for rapid, non-invasive analysis addressing the limitations of traditional methods. The present work primarily focuses on the evaluation of RS combined with predictive ML models in a non-real-time setting. Our goal is to adapt these techniques for future application in real-time monitoring and determination of yeast viability in biotechnological processes. We demonstrate that RS, in combination with ML, is a promising tool for non-invasive inline monitoring of fermentation processes.

Keywords: process analytical technology (PAT); yeast viability; fermentation process; Raman spectroscopy; machine learning

check for updates

Citation: Heese, R.; Wetschky, J.; Rohmer, C.; Bailer, S.M.; Bortz, M. Fast and Non-Invasive Evaluation of Yeast Viability in Fermentation Processes Using Raman Spectroscopy and Machine Learning. *Beverages* **2023**, *9*, 68. https://doi.org/10.3390/beverages9030068

Academic Editors: Antonio Morata, António Manuel Jordão, Fernanda Cosme and Ileana Vigentini

Received: 29 June 2023
Revised: 3 August 2023
Accepted: 14 August 2023
Published: 18 August 2023

1. Introduction

Beer, wine, cider, and other alcoholic beverages have been part of our civilization for thousands of years even before their scientific underpinnings were fully understood. It was only in the 19th century that Louis Pasteur was able to prove that yeast is an essential driver in alcoholic fermentation [1]. Ethanol production is primarily a consequence of anaerobic conditions created by rapid yeast growth along with increasing nutrient and sugar limitations; this eventually leads to active fermentation metabolism and, finally, increased ethanol production [2]. In most instances, yeast strains currently used in industrial fermentation processes at breweries and wineries belong to the *Saccharomyces cerevisiae* (*S. cerevisiae*) species. This yeast species is highly efficient in the alcoholic fermentation processes due to its ability to convert sugar into ethanol, its high fermentation power, and adaptability to changing conditions during biotechnological use [3]. After many years of classical industrial production, where process parameters are monitored offline and require sampling as well as time-consuming analytical methods, the industry is now rapidly moving toward digital transformation. Automated and digitalized processes allow for a fully controlled, flexible, and highly efficient production process that ensures high-quality products. This not only results in a standardized and cost-efficient production but also reduces process-associated risks.

Increasingly, inline process analytical technologies (PATs) are applied for real-time and in situ monitoring of parameters, such as pH, temperature, and dissolved oxygen. Thereby, large amounts of data are collected that feed into the mathematical modeling of processes, their prediction, and control. In high-value fields like biopharmaceutical production, PAT is gradually replacing traditional standard physical sensors within reactors [4], suggesting its potential use in other biotechnological processes, such as alcoholic fermentation.

At present, the production of alcoholic beverages requires monitoring yeast viability, cell count, and growth behavior in order to ensure a controlled, constant, and reproducible fermentation process [5]. State-of-the-art technologies to determine the number of viable and non-viable cells include classical colony counting to determine the number of viable cells. Non-viable cells are often determined by staining techniques using dyes like methylene blue and slide culture procedures [6–8]. However, these microbiological techniques are time-consuming and error-prone (e.g., they suffer from false positive results due to long exposure times and subjective evaluations). Hence, there is a strong need for a fast, non-invasive, and non-biased method to evaluate yeast cell viability during fermentation processes to ensure high-quality products and prevent microbiological contamination.

Spectroscopical methods like Raman spectroscopy (RS) are very powerful tools for the identification, quantification, and monitoring of metabolites or materials amenable to non-invasive, real-time, and inline measurements, while avoiding sample preparation. For example, non-invasive inline RS measurements are already being utilized in feedback control systems to improve ethanol production, which enables the real-time quantitative analysis of glucose and ethanol during *S. cerevisiae* fermentation [9–11]. Beyond that, RS has the potential to serve as a powerful tool to identify, quantify, and monitor microbes, representing a valuable technology for inline measurements of fermentation processes [12]. Namely, RS provides detailed information on the molecular level, a "fingerprint" that enables the discrimination of closely related bacteria or the identification of bacterial contaminants in food products based on the analysis of Raman spectral differences [13–18]. Several studies have been performed to evaluate the application of Raman imaging, e.g., for food quality and safety control [19–21]. Yet, while non-destructive and highly precise [18], limited data exist for Raman-based methods for monitoring yeast in biotechnological brewing processes. The present work, therefore, focuses on the initial evaluation of the effectiveness of RS combined with predictive machine learning (ML) models for prospective real-time monitoring and determination of yeast viability in biotechnological processes.

In this study, we obtained spectroscopic datasets of viable and heat-inactivated yeast cells of different species and cultured them in different media to train ML models. Six ML approaches were considered and their viability prediction performances were compared in terms of the balanced accuracy (i.e., normalized values between zero and one, with the latter representing 100% prediction accuracy). Furthermore, the influence of artificially added noise on prediction accuracy was investigated to estimate the impact of imperfections in actual ex vitro measurements.

2. Materials and Methods

2.1. Organisms and Growth Media

Two yeast strains used in this study, *S. cerevisiae* (ATCC 18824) and *Dekkera bruxellensis* (*Dekkera bruxellensis* (*D. bruxellensis*)), formerly labeled as *Brettanomyces bruxellensis*, were purchased from *ATCC* (Manassas, VA, USA) and *White Labs Brewing Co.* (San Diego, CA, USA), respectively. Yeast extract peptone dextrose (YPD) culture medium (20 g L^{-1} peptone, 10 g L^{-1} yeast extract, and 20 g L^{-1} glucose) were used for yeast cultivation. Yeast culture was inoculated to a ratio of 1:500 in YPD medium followed by incubation at 32 °C and 170 rpm for 20 h or 72 h, respectively. These timespans were chosen due to laboratory practicability and monitoring over time. For RS analysis, additional media (commercially available beer and apple juice) were purchased and sterile-filtered (0.22 µm pore size). Ultrapure H_2O (*Milli-Q*) was used as the negative control.

2.2. Sample Preparation for Raman Spectroscopy

For sample preparation, grown cultures of *S. cerevisiae* and *D. bruxellensis* were pelleted by centrifugation (5000× *g*, 5 min), washed with H_2O, and adjusted to an optical density (OD600) of 10 to ensure a constant amount of cells in each sample. For *S. cerevisiae*, 1 mL of culture was incubated at 72 °C for 10 min followed by incubation on ice for one minute (referred to as "heat-inactivated" in the following sections). Additionally, 1 mL of each sample was kept at 32 °C, followed by incubation on ice for one minute (referred to as "viable" in the following sections). For different media tested, *S. cerevisiae* cultures grown in YPD were mixed with either sterile-filtered beer, apple juice, or water, and adjusted to an optical density (OD600) of 10. For mixed samples, yeast cultures of *S. cerevisiae* and *D. bruxellensis* (considered as artificial contamination) were adjusted to an OD600 value of 10 in H_2O followed by mixtures in different ratios, as stated in the following section. From each sample produced, 20 µL were applied to lime soda slides (*Carl Roth*), followed by air fixation for spectroscopic analysis.

2.3. Raman Spectroscopy

The RS analysis of samples was performed using an *inViaTM Quontor Raman spectroscope* (*Renishaw plc*, *Wotton-under-Edge*, United Kingdom). Raman spectra of 50 to 60 randomly selected yeast cells of several sections in each sample were obtained using a 100× dry objective (0.85 NA) with a 45 W 532 nm laser adjusted to an intensity of 10% and 1 s exposure. To reduce background noise, each measurement was accumulated ten times for each cell. Raw data acquisition was obtained in a spectral detection range of 283 cm^{-1} to 2016 cm^{-1}. The scattered radiation was passed through a notch filter, focused onto a monochromator with 1800 lines mm^{-1} grating, and detected by a *Peltier*-cooled CCD camera (1024 pixel × 256-pixel sensor).

2.4. Dataset Composition

Acquired datasets of *S. cerevisiae* were categorized into 10 different groups, depending on the condition (viable, heat-inactivated), background media (YPD, beer, apple, juice and H_2O) and different time points of the measurements (20 h and 72 h) for the analysis, as listed in Tables 1 and 2. In addition, two mixed-sample models were produced to simulate more realistic conditions, as listed in Table 3. Mixed samples were composed as follows: The first set of samples consisted of 33% viable and 33% heat-inactivated *S. cerevisiae* cells mixed with 33% viable *D. bruxellensis* culture for equal distribution. The second set of samples consisted of 75% viable and 20% heat-inactivated *S. cerevisiae* culture mixed with 5% viable *D. bruxellensis* culture. Since *D. bruxellensis* shows, to some extent, similarity to *S. cerevisiae* on the sequence level [22], it is suitable to demonstrate the contamination of a sample with a related yeast strain. With respect to *S. cerevisiae*, the second mixture is mostly heat-inactivated, whereas the first mixture contains the same ratio of viable and heat-inactivated cells. In the scope of this work, we consider the first mixture as viable and the second as heat-inactivated.

Table 1. Total numbers of Raman spectra obtained from *S. cerevisiae* samples (viable or heat-inactivated) in water (control). The corresponding dataset `H2O` was used for the ML task.

Yeast Strain	Media (Background)	Viable Samples	Heat-Inactivated Samples	Dataset
S. cerevisiae	H_2O	362	360	`H2O`

Table 2. Total Raman spectra numbers obtained from *S. cerevisiae* samples in different media in analogy to Table 1.

Yeast Strain	Media (Background)	Viable Samples	Heat-Inactivated Samples	Dataset
S. cerevisiae	Apple juice	120	180	`Apple`
	Beer	120	183	`Beer`
	YPD 20 h	1127	1194	`YPD-20`
	YPD 72 h	120	180	`YPD-72`

Table 3. Total numbers of Raman spectra obtained from mixture samples in analogy to Table 1.

Yeast Strain	Media (Background)	Samples	Dataset
First mixture [1] (more heat-inactivated *S. cerevisiae*)	H_2O	1004	`Mix`
Second mixture [2] (more viable *S. cerevisiae*)	H_2O	708	

[1] Composition: 33% viable *S. cerevisiae*, 33% heat-inactivated *S. cerevisiae*, and 33% viable *D. bruxellensis*. [2] Composition: 75% viable *S. cerevisiae*, 20% heat-inactivated *S. cerevisiae*, and 5% viable *D. bruxellensis*.

3. Machine Learning Methods

As presented in Tables 1–3, we considered six datasets, which were compiled from the RS experiments: `H2O`, `Apple`, `Beer`, `YPD-20`, `YPD-72`, `Mix`. Additionally, we combined all datasets into a joint dataset `All`. Each dataset consists of spectroscopic data of yeast samples, which are either viable or inactivated by heat. For the `Mix` dataset, we considered the second mixture with 708 measurements as viable (since the majority of *S. cerevisiae* in the mixture is viable) and the first mixture with 1004 measurements as heat-inactivated.

To summarize, the practically relevant goal was to identify the binary viability of yeast (viable/heat-inactivated) from the spectroscopic data by means of pattern recognition: a well-defined classification problem. That is, the ML task was to assign a class label—either viable or heat-inactivated—for Raman spectra obtained from each single yeast cell measured in the samples. In other words, we searched for an algorithm that allows the mapping

$$\text{Raman spectrum} \rightarrow \text{binary yeast viability} \tag{1}$$

such that an RS of a yeast sample is sufficient for identifying its viability.

In the following, we first describe the data-processing pipeline that has allowed us to cast the raw measurement data into a suitable form. Since we only performed in vitro measurements, we also included a noising process in our pipeline that allowed us to induce artificial noise to emulate a less ideal (i.e., ex vitro) scenario. In other words, we considered the artificially induced noise as the presumed influence of potential ex vitro measurements on the data in contrast to data from the actually performed in vitro measurements. Our data-processing pipeline fully defines our classification problem. Subsequently, we briefly describe the ML models that we use to solve this problem.

3.1. Data Processing Pipeline

Each raw dataset $\mathbf{D} := \{\mathbf{d}^1, \ldots, \mathbf{d}^N\}$ consists of N data points of the form $\mathbf{d}^n := (\mathbf{K}^n, \mathbf{I}^n)$, which are composed of a vector of wave numbers $\mathbf{K}^n \in \mathbb{R}_+^{1015}$ and a vector of corresponding intensities $\mathbf{I}^n \in \mathbb{R}^{1015}$ for $n \in \{1, \ldots, N\}$. Furthermore, each dataset $\mathbf{D}$ is associated with a yeast viability label $y \in \{0, 1\}$, where 1 represents viable and 0 represents heat-inactivated yeast. These labels constitute the ground truth. The wave numbers were measured in the range of 283 cm^{-1} to 2016 cm^{-1}, whereas the corresponding intensities were measured in arbitrary detector units.

First, we performed a preprocessing of the data to transform it into a unified form that is suitable for ML applications. For each data point n, five preprocessing steps were used. We

1. Interpolated the intensities uniformly, such that they spanned the same wavelength domain.
2. Rescaled the intensities to the unit interval.
3. Fixed a systematic error in the measurement results by linear interpolation for wavelengths in the range of 830.437 cm^{-1} to 864.667 cm^{-1}. This systematic error is a direct result of the hardware used in the experimental setup.
4. Performed a baseline correction.
5. Performed a standardization of the intensities.

To simplify the notation, we omit all measurement units in the following. A detailed description and formal definition of the data-processing pipeline can be found in Appendix A. For data point n, the resulting vector of wave numbers and the corresponding intensity vector are denoted by $\tilde{\mathbf{K}}$ and $\tilde{\mathbf{I}}^n$, respectively. In Appendix B, we show the mean $\mathbb{E}_n\, \tilde{I}_i^n$ and standard deviation $\mathbb{V}_n\, \tilde{I}_i^n$ of each preprocessed dataset, divided into data for $y = 1$ (viable) and $y = 0$ (heat-inactivated) to emphasize the differences.

To simulate the effects of ex vitro measurements, we also considered data, which have been perturbed by artificially generated noise. As formally described in Appendix A, the absolute noise level is controlled by a parameter $\sigma > 0$ that can be chosen at will. The resulting intensity vector for data point n is denoted by $\tilde{\mathbf{I}}^n(\sigma)$. We performed a perturbation for all datasets for different values of $\sigma \in [0, 0.05]$. The signal-to-noise ratio decreases as the perturbation σ increases, as visualized in Appendix B.

3.2. Classification Models

Formally, our goal was to predict the yeast viability $y \in \{0, 1\}$ (viable or heat-inactivated) from the measured Raman spectrum $\tilde{\mathbf{I}}$. This corresponds to the classification problem

$$M : \mathbb{R}^{1015} \to \{0, 1\} \tag{2}$$

as a formal representation of (1) mapping from features $\tilde{\mathbf{I}}$ to class labels y. For this purpose, we propose five well-known ML approaches to solve this problem and comparatively discuss their performances.

These approaches were chosen to represent conceptually different strategies [23,24]. The first three approaches constitute different kinds of ensemble methods based on a collection of decision trees. An ensemble method combines a set of models with the goal of creating a new model with better performance than the individual models from the set. In our case, the individual models are decision trees. Each decision tree consists of a set of binary decisions (i.e., inequalities for single features) that are traversed in a tree-like fashion to predict class labels. The fourth approach is a variant of Bayesian inference, whereas the last two approaches are established standard methods based on the optimization of a loss function. Specifically, we consider the following six ML approaches:

1. Random forest classifier (RF) [25]. An RF is an ensemble method based on decision trees, where each tree is trained on a random subset of the training dataset to enable diversification and reduce overfitting. This ensemble strategy is also known as "bagging". The average of all decision tree predictions decides the resulting class label prediction for the random forest classifier.
2. Gradient boosting classifier (GB) [26]. A GB is an ensemble method based on decision trees similar to an RF. However, instead of relying on randomized diversification, an ensemble strategy known as "boosting" is used. This strategy iteratively adds decision trees to the ensemble with the goal of improving the resulting prediction.

This strategy can lead to better overall models but is more vulnerable to overfitting than an RF.

3. EXtreme Gradient Boosting classifier (XGB) [27]. An XGB is an extension of a GB that includes various improvements with the goal of pushing gradient boosting to its limits. However, it is not guaranteed that XGB generally performs better than GB; therefore, we consider both approaches.
4. Gaussian process classifier (GPC) [28]. A GPC is based on Bayesian inference, where a Gaussian process is used as a prior probability distribution. Such a Gaussian process is defined by a collection of random variables with a joint Gaussian distribution. Due to the Bayesian premise, the resulting model allows to assign an uncertainty to each class label prediction.
5. Support vector machine classifier (SVM) [29,30]. An SVM is determined by the solution of an optimization problem with the goal of finding a hyperplane in the feature space that best distinguishes the class labels. We use a (radial basis function) kernel machine that maps the feature into a higher-dimensional space to enable non-linear separation.
6. Neural network (NN) [31]. A NN consists of a set of layers, each of which maps its input to an output based on a predefined functional dependency that is determined by a set of trainable parameters. The features constitute the input for the first layer and the output of the last layer determines the class label predictions. A gradient-based learning algorithm is used to optimize a loss function with the goal of choosing trainable parameters that achieve the best class label prediction for the training data. Neural networks are highly generic models that can be customized in many ways due to their modular structure. However, this customization capability is, at the same time, a challenge, as good architecture (i.e., design of layers) is not always obvious. For this reason, we use a neural architecture search (NAS) algorithm to also optimize the architecture of the neural network in addition to its parameters. Specifically, we consider architectures with and without one-dimensional convolutions that are typically used for data in the form of time series.

In Appendix C, we specify the details and parameters of the presented models. For further reading, we refer to the cited references and references therein.

4. Results

In the current section, we present our numerical results for the yeast viability classification task. We start with a proof of concept and consider the basic in vitro scenario for yeast in water, which only involves the `H2O` dataset without artificial noise. Subsequently, we show how well the proposed ML approaches perform in other media. Next, we study the effect of mixtures of different yeast strains representing artificial contamination within a sample and its influence on the model performances. Finally, we present the effect of artificially imposed noise within our data-processing pipeline on the model performances using different media and mixtures.

4.1. Proof of Concept: Predicting Yeast Viability

As a first study, we considered the `H2O` dataset as described in Section 3, which is based on Raman spectra of *S. cerevisiae* in water (control) and free of artificial background noise. In total, 722 Raman spectra were available for training and analysis purposes according to Table 1. Based on this data, we evaluated how six different ML approaches performed on the classification problem from (2). For each approach, we trained on the preprocessed `H2O` dataset with a 10-fold cross-validation setup. That is, we split the dataset into 10 parts (further referred to as "chunks") of approximately the same size. Here, and in the following, we used a so-called "stratified" approach, such that approximately the same ratio of viable and heat-inactivated samples are present in each split. The models were then trained independently on nine out of the 10 chunks, leaving one chunk remaining for testing purposes. Consequently, each data point was used nine times as training data and once as test data for each model. The ten training runs resulted in ten classifiers for each ML approach.

In Table 4 and Figure 1, we present the *balanced accuracies* of all ML approaches, evaluated on the test dataset. The balanced accuracy represents the fraction of correct predictions over all samples weighted by the respective amount of samples for each class, such that class imbalances are accounted for [32]. This compensates for the fact that we have slightly fewer heat-inactivated samples than viable samples in the dataset. The balanced accuracy can attain values between 0 (worst, i.e., all predictions are wrong) and 1 (best, i.e., all predictions are correct), where a value of 0.5 is the score of a random guess. For each ML approach, we obtained ten balanced accuracies based on the ten different data splits and could, therefore, determine the corresponding means and standard deviations.

As listed in Table 4, we found in our study that the balanced accuracy ranges from 0.76 ± 0.03 for NN to 0.84 ± 0.03 for SVM. The remaining models achieved a balanced accuracy of 0.82 ± 0.03 and 0.81 ± 0.02, respectively.

Table 4. Test performances of classifiers with the task to predict the viability of yeast in water. All models were trained and evaluated on the `H2O` dataset. We used 10-fold cross-validation for each model and show the mean and standard deviation of the balanced accuracy. These results are also plotted in Figure 1. The best results are highlighted in bold type.

Training Data	Test Data	Model	Balanced Accuracy
`H2O`	`H2O`	RF	0.82 ± 0.03
		GB	0.82 ± 0.03
		XGB	0.81 ± 0.02
		GPC	0.82 ± 0.03
		SVM	**0.84 ± 0.03**
		NN	0.76 ± 0.03

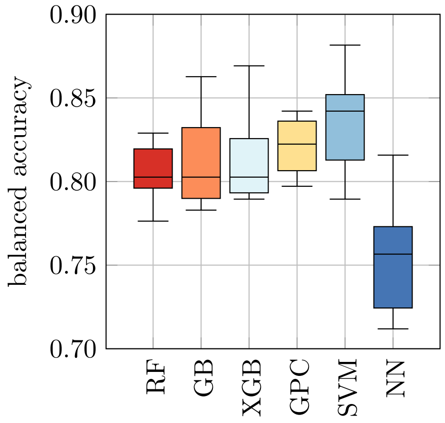

Figure 1. Test performances of classifiers for yeast viability prediction on the `H2O` dataset in the form of boxplots. These results are also listed in Table 4.

4.2. Yeast Viability in Different Media

In the next step, we evaluated the performance of the models trained on the `H2O` dataset predicting yeast viability in other media, i.e., the `Apple`, `Beer`, `YPD-20`, and `YPD-72` datasets. As listed in Table 2, these datasets originate from *S. cerevisiae* in YPD, beer, and apple juice, as viable or heat-inactivated samples, respectively. Additionally, for YPD, two different time points (20 and 72 h) are used. Our ML models of interest are all classifiers that were trained on *S. cerevisiae* in H_2O (control) with 10-fold cross-validation, as presented in Section 4.1. That is, we have ten trained classifiers for each ML approach.

As a first numerical experiment, we used the datasets `Apple`, `Beer`, `YPD-20`, and `YPD-72` as inputs for each of these trained models and predicted the class labels (without retraining), i.e., we used the models that were trained only with Raman spectra of yeast in water to predict the viability of yeast in other media. Based on these predictions, we evaluated the balanced accuracy. The results are presented in Table 5 (a) and Figure 2. We found that previously trained classifiers showed a rather poor performance on yeast in other media, ranging from 0.49 ± 0.00 for RF, GB, XGB, and SVM on `YPD-20` to 0.60 ± 0.01 for SVM on `Apple`. We recall that a balanced accuracy of 0.5 corresponds to a random guess. Hence, these results indicate that the application of ML models that have only been trained on control samples (i.e., *S. cerevisiae* in water) are not suitable for the discrimination of viable and heat-inactivated yeast cells in other media. Consequently, it seems mandatory for practical applications to train individual ML models for each background medium of interest.

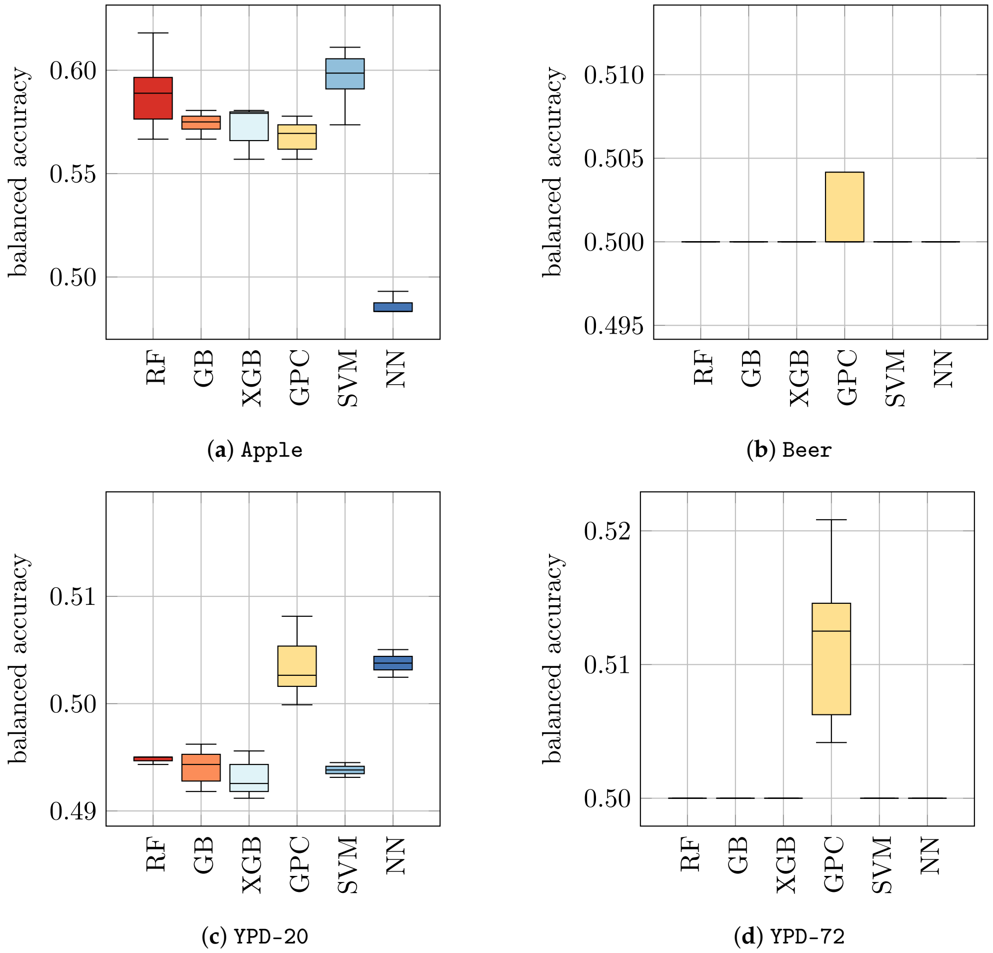

(**a**) `Apple`

(**b**) `Beer`

(**c**) `YPD-20`

(**d**) `YPD-72`

Figure 2. Test performances of classifiers trained on `H2O` for yeast viability prediction in other media. The results are also listed in Table 5 (a).

As a consequence of these findings, we trained new models on each dataset separately, following the approach detailed in Section 4.1. That is, we considered the same four datasets as before (`Apple`, `Beer`, `YPD-20`, and `YPD-72`) and trained ten classifiers on each dataset for each ML approach using 10-fold cross-validation. With this approach, we checked if the predictive performance could be increased with different data. The results are presented in Table 5 (b) and Figure 3. Indeed, we found that for all datasets tested in this approach, the performances of ML models significantly improved compared to models that were only trained on `H2O`. The resulting balanced accuracy ranged from 0.73 ± 0.05 for NN on `Beer` to 0.97 ± 0.03 for GPC and SVM on `Apple`. To enable a better comparison, we show the balanced accuracies of classifiers trained on datasets with yeast in media as solid boxplots in Figure 3, whereas the classifiers from Figure 2 (that were trained on `H2O`) are displayed opaquely.

Table 5. Test performance of classifiers with the task of predicting the viability of yeast in different media. We show the mean and standard deviation in analogy to Table 4. These results are also plotted in Figures 2 and 3, respectively. The best results are highlighted in bold type.

(a) Trained on `H2O`, evaluated on `Apple`, `Beer`, `YPD-20` and `YPD-72`, respectively.

Training Data	Test Data	Model	Balanced Accuracy
`H2O`	`Apple`	RF	0.59 ± 0.01
		GB	0.58 ± 0.01
		XGB	0.58 ± 0.02
		GPC	0.57 ± 0.01
		SVM	**0.60** ± **0.01**
		NN	0.49 ± 0.00
`H2O`	`Beer`	**RF**	**0.50** ± **0.00**
		GB	**0.50** ± **0.00**
		XGB	**0.50** ± **0.00**
		GPC	**0.50** ± **0.00**
		SVM	**0.50** ± **0.00**
		NN	**0.50** ± **0.00**
`H2O`	`YPD-20`	RF	0.49 ± 0.00
		GB	0.49 ± 0.00
		XGB	0.49 ± 0.00
		GPC	**0.50** ± **0.00**
		SVM	0.49 ± 0.00
		NN	**0.50** ± **0.00**
`H2O`	`YPD-72`	RF	0.50 ± 0.00
		GB	0.50 ± 0.00
		XGB	0.50 ± 0.00
		GPC	**0.51** ± **0.01**
		SVM	0.50 ± 0.00
		NN	0.50 ± 0.00

(b) Trained and evaluated on `Apple`, `Beer`, `YPD-20`, and `YPD-72`, respectively.

Training Data	Test Data	Model	Balanced Accuracy
`Apple`	`Apple`	RF	0.91 ± 0.05
		GB	0.89 ± 0.06
		XGB	0.86 ± 0.05
		GPC	**0.97** ± **0.03**
		SVM	**0.97** ± **0.03**
		NN	0.83 ± 0.08
`Beer`	`Beer`	RF	0.91 ± 0.05
		GB	0.88 ± 0.06
		XGB	0.86 ± 0.06
		GPC	0.89 ± 0.06
		SVM	**0.94** ± **0.05**
		NN	0.73 ± 0.05
`YPD-20`	`YPD-20`	RF	0.94 ± 0.01
		GB	0.94 ± 0.01
		XGB	0.93 ± 0.02
		GPC	**0.96** ± **0.01**
		SVM	0.94 ± 0.01
		NN	0.83 ± 0.11
`YPD-72`	`YPD-72`	RF	0.88 ± 0.08
		GB	**0.90** ± **0.06**
		XGB	0.89 ± 0.07
		GPC	**0.90** ± **0.06**
		SVM	0.86 ± 0.08
		NN	0.81 ± 0.12

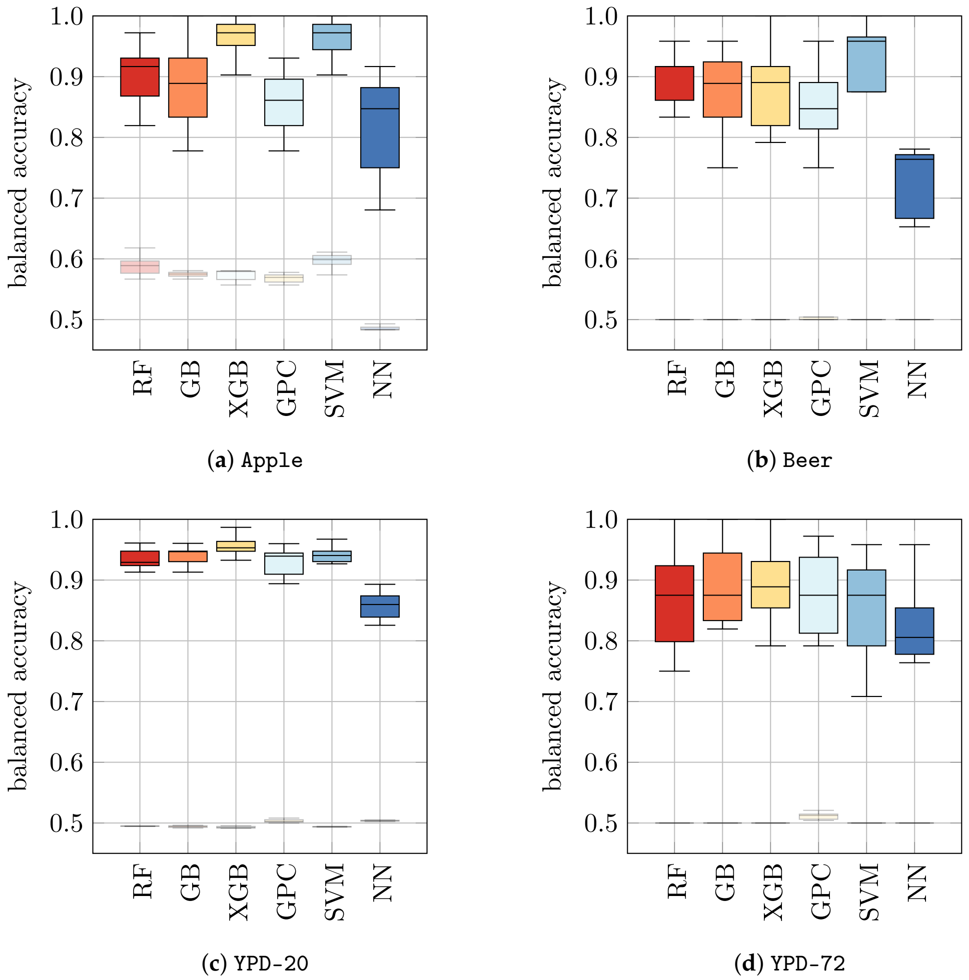

(**a**) `Apple`

(**b**) `Beer`

(**c**) `YPD-20`

(**d**) `YPD-72`

Figure 3. Test performances of classifiers with the task to predict the viability of yeast in different media. The solid boxplots show the test performances of all models of the respective datasets for 10-fold cross-validation. These results are also listed in Table 5 (b). For comparison, the opaque boxplots show the performances of the 10-fold models trained on `H2O` for the respective datasets, i.e., the results plotted in Figure 2.

4.3. Viability of Mixed Strains

The previously obtained results raise the question as to whether ML approaches are also able to discriminate viable from heat-inactivated *S. cerevisiae* if other yeast strains are present in the sample. To study this question, cultures of *D. bruxellensis*—which is known as an undesired organism in wine production—were cultivated in YPD, followed by resuspension in water. Samples containing additional amounts of viable and heat-inactivated *S. cerevisiae* lead to the dataset `Mix`, as listed in Table 3.

In analogy to Section 4.2, we pursued two approaches. First, we used the classifiers that were trained on `H2O` and use `Mix` as input. Based on the predictions, we evaluated the balanced accuracy to determine if the classification also works for mixtures without having appropriate data in the training dataset. Second, we directly trained classifiers on `Mix` using 10-fold cross-validation in analogy to Section 4.1 and evaluated the balanced accuracy. The results are presented in Table 6 and Figure 4. In both cases, ML approaches led to a relatively low balanced accuracy for the mixed samples. In the first case, the balanced accuracy ranged from 0.47 ± 0.01 for NN to 0.50 ± 0.01 for RF, whereas in the second case, it ranged from 0.54 ± 0.04 for NN to 0.56 ± 0.03 for GPC.

Table 6. Test performances of classifiers with the task to predict the viability of yeast in a mixture of different yeast strains. We show the mean and standard deviation in analogy to Table 4. These results are also plotted in Figure 4. The best results are highlighted in bold type.

(a) Trained on `H2O`, evaluated on `Mix`.

Training Data	Test Data	Model	Balanced Accuracy
`H2O`	`Mix`	**RF**	**0.50 ± 0.01**
		GB	0.49 ± 0.01
		XGB	0.49 ± 0.01
		GPC	0.48 ± 0.01
		SVM	0.49 ± 0.01
		NN	0.47 ± 0.01

(b) Trained and evaluated on `Mix`.

Training Data	Test Data	Model	Balanced Accuracy
`Mix`	`Mix`	RF	0.50 ± 0.01
		GB	0.55 ± 0.03
		XGB	0.55 ± 0.04
		GPC	**0.56 ± 0.03**
		SVM	0.55 ± 0.03
		NN	0.54 ± 0.04

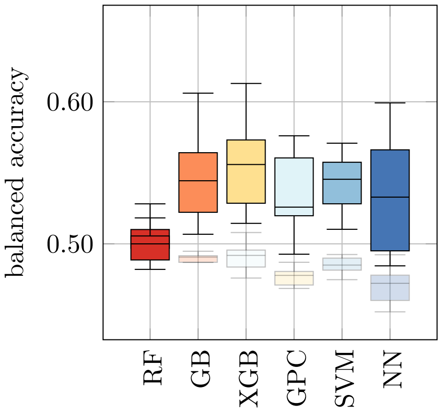

Figure 4. Test performances of classifiers for yeast viability prediction given mixtures of yeast strains. The solid boxplots show the test performances of all models for 10-fold cross-validation that were trained and evaluated on `Mix`. These results are also listed in Table 6 (b). For comparison, the opaque boxplots show the performances of the 10-fold models trained on `H2O`, i.e., the results listed in Table 6 (a).

As an alternative approach, we combined all datasets from this study into a new dataset: `All`. Again, in analogy to Section 4.1, we trained and evaluated all ML approaches on this dataset using 10-fold cross-validation. The results are shown in Table 7 and Figure 5. We found that this approach revealed slightly increased balanced accuracy in comparison to the results from Table 6 and Figure 4, but a decreased score in comparison to the results from Table 5 (b) and Figure 3. The balanced accuracy ranges from 0.70 ± 0.02 for NN to 0.73 ± 0.01 for GPC and 0.73 ± 0.02 for SVM.

Table 7. Test performances of classifiers with the task to predict the viability of yeast for different media or mixtures. All models were trained and evaluated on the `All` dataset. We show the mean and standard deviation in analogy to Table 4. These results are also plotted in Figure 5. The best results are highlighted in bold type.

Training Data	Test Data	Model	Balanced Accuracy
`All`	`All`	RF	0.71 ± 0.02
		GB	0.72 ± 0.02
		XGB	0.72 ± 0.03
		GPC	**0.73** ± **0.01**
		SVM	**0.73** ± **0.02**
		NN	0.70 ± 0.02

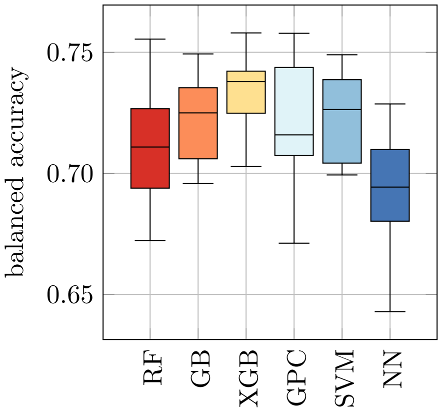

Figure 5. Test performances of classifiers for yeast viability prediction given different media and mixtures using the `All` dataset. The results are also listed in Table 7.

4.4. Yeast Viability under Artificial Noise

In a final study, we compare the model performance using all datasets with artificially imposed noise, as defined in Section 3. To summarize, we presume that, in our simple approach, the noise represents the imperfections of an ex vitro measurement. The absolute noise level is controlled by a parameter $\sigma > 0$, i.e., the larger the σ, the noisier the ex vitro environment in which the measurements take place, as visualized in Appendix B. The results are shown in Figure 6.

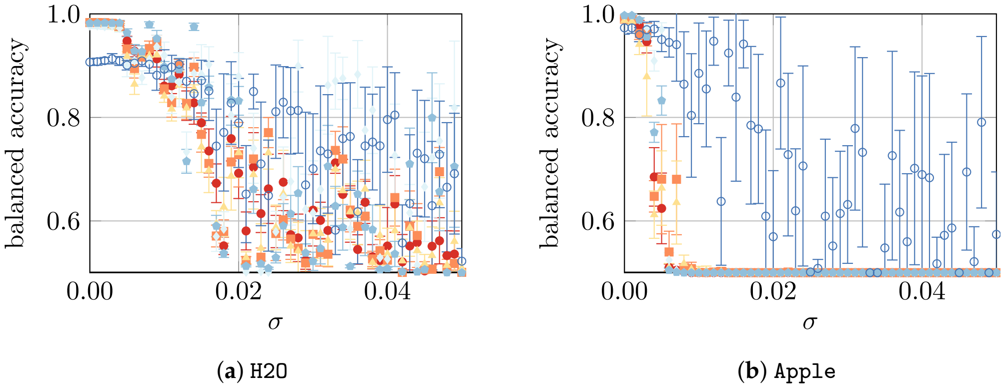

(**a**) `H2O` (**b**) `Apple`

Figure 6. *Cont.*

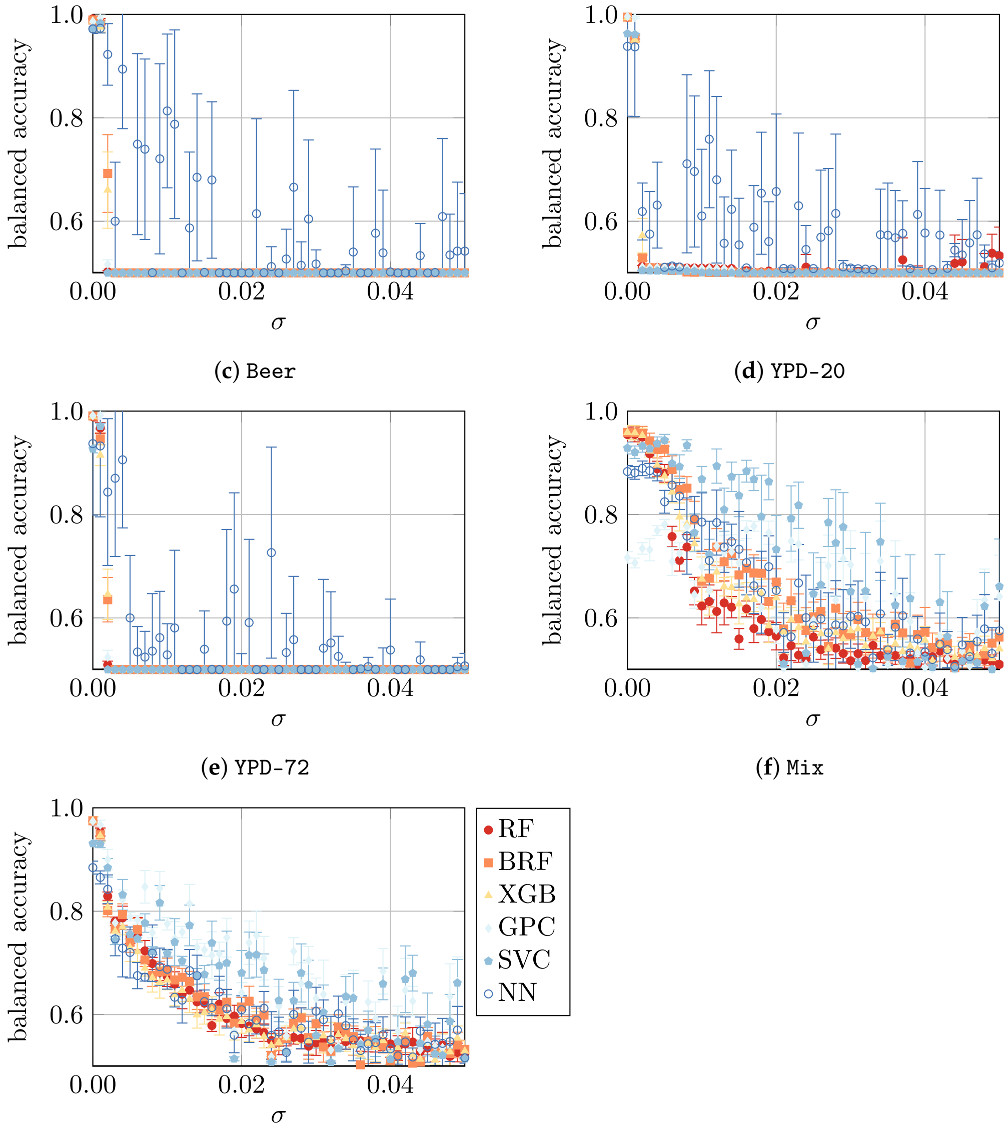

(**c**) `Beer`

(**d**) `YPD-20`

(**e**) `YPD-72`

(**f**) `Mix`

(**g**) `All`

Figure 6. Test performances of all models of the respective datasets for 10-fold cross-validation. We show markers at mean values; the error bars represent one standard deviation. The results for $\sigma = 0$ are also listed in Table 5 (b).

4.5. Comparison of Machine Learning Models

In the previous sections, we trained and tested our ML models of interest on various datasets and have found that the resulting balanced accuracies are mostly in similar ranges. To obtain a better understanding of the competitive performance of the models, we performed a pairwise statistical comparison [33]. For this purpose, we performed Welch's t-test [34] of the score of every model versus every other for each test and training dataset combination (without artificially imposed noise, i.e., $\sigma = 0$). That is, for each test and training dataset combination, we evaluated $\binom{6}{2} = 15$ statistical tests using the respective 10 balanced accuracies that have been obtained from the 10-fold cross-validation for every model. We considered a model superior to another in a statistically significant way if its mean balanced accuracy is larger and the p-value from the corresponding test is smaller than 0.05. For larger p-values, no statistically significant superiority relation can be established. Our test can be considered as an indicator of superiority but might not be statistically conclusive because of the limited amount of data considered in this experiment.

Since we are only interested in models that perform reasonably well, we limit the comparison to models with a mean balanced accuracy of at least 0.7. This rule excludes all models from Tables 5 (a) and 6. The result is presented in Table 8, where we list the superior models (and their respective inferior models) for each test and training dataset combination from Tables 4, 5 (b), and 7. To summarize, we find that GPC is a superior model for every listed test and training dataset combination. Hence, we consider it as the best overall model for our use case. On the other hand, NN was inferior in all cases and can, therefore, be considered as a less-suited model.

Table 8. Model comparison of the results from Tables 4, 5 (b) and 7. A model is superior to another if its mean balanced accuracy is larger and Welch's *t*-test (with respect to the balanced accuracies from the 10-fold cross-validation) yields a *p*-value larger than 0.05. The list is limited to models with a mean balanced accuracy of at least 0.7. The best results are highlighted in bold type.

Training Data	Test Data	Superior Model	Inferior Models	Superior Model Balanced Accuracy
H2O	H2O	RF	NN	0.82 ± 0.03
		GB	NN	0.82 ± 0.03
		XGB	NN	0.81 ± 0.02
		GPC	NN	0.82 ± 0.03
		SVM	NN	**0.84** ± **0.03**
Apple	Apple	RF	XGB, NN	0.91 ± 0.05
		GPC	RF, GB, XGB, NN	**0.97** ± **0.03**
		SVM	RF, GB, XGB, NN	**0.97** ± **0.03**
Beer	Beer	RF	NN	0.91 ± 0.05
		GB	NN	0.88 ± 0.06
		XGB	NN	0.86 ± 0.06
		GPC	NN	0.89 ± 0.06
		SVM	GB, XGB, NN	**0.94** ± **0.05**
YPD-20	YPD-20	RF	NN	0.94 ± 0.01
		GB	NN	0.94 ± 0.01
		XGB	NN	0.93 ± 0.02
		GPC	RF, GB, XGB, SVM, NN	**0.96** ± **0.01**
		SVM	NN	0.94 ± 0.01
YPD-72	YPD-72	**GPC**	NN	**0.90** ± **0.06**
All	All	GB	NN	0.72 ± 0.02
		XGB	NN	0.72 ± 0.03
		GPC	RF, NN	**0.73** ± **0.01**
		SVM	NN	**0.73** ± **0.02**

5. Discussion

In this study, we combined RS with predictive ML models to evaluate the prospective real-time monitoring of yeast viability in a biotechnological setting. To this end, six ML approaches (RF, GB, XGB, GPC, SVM, and NN—for a detailed description, see Section 3.2) were trained and tested on various datasets obtained from in vitro RS measurements with the goal of evaluating their performances. The measurements were performed on yeast in different background media and a mixed setting. As summarized in the following, our study is divided into four parts.

In the first part of the study, we considered a viability prediction for yeast in water (control). The resulting mean balanced accuracies (higher is better) are similar for five ML approaches, ranging from 0.81 for XGB to 0.84 for SVM, where only NN performed significantly worse with 0.76. Despite the small dataset of only 722 spectra to analyze, the reasonably good predictive performances of most approaches validate our proof-of-concept for the prediction of yeast viability in an in vitro scenario.

In the second part of the study, we considered yeast that was prepared in background media other than water. Our results revealed that ML models trained on water samples showed comparatively low performance when applied to datasets obtained from yeast in different media. With balanced accuracy values around 0.5, which corresponds to a random guess, the transfer of models trained on water to other media and mixtures is considered not applicable. However, the direct training of ML models on the respective datasets of yeast in media revealed a highly improved balanced accuracy that is comparable to a water medium. Furthermore, combining all datasets for ML training did not yield good, balanced accuracy scores as separate training and prediction for each medium. These findings clearly show the great influence of the background media used for yeast cultivation, reflecting more realistic conditions in biotechnological processes.

In the third part of the study, we considered the contamination with an undesired strain, such as *D. bruxellensis* yeast that occurs during wine production. For this purpose, samples were spiked with this artificial contaminant. The analysis yielded poor results for the predictive capabilities of ML models on such data, showing a balanced accuracy that is only slightly above 0.5. However, we cannot rule out that the poor performance is due to the experimental setup, as the spiked samples were made in the `H2O` background.

Finally, in the fourth part of the study, we considered artificially imposed noise on the data. As expected, such noise led to a decrease in model performance for all datasets. For the `Beer`, `Apple`, `YPD-20`, and `YPD-72` datasets, the performance drops (almost) immediately, whereas for the `H2O`, `Mix`, and `All` datasets, a slower decline was observed. For `Apple`, `Beer`, `YPD-20`, and `YPD-72`, NN is the most resilient ML approach that can—in some very noisy cases—lead to a model with reasonably good performance. Similarly, for `Mix` and `All`, the three approaches—GPC, SVM, and NN—are the most resilient ones. Finally, the most resilient approaches for `H2O` are GPC and SVM. In summary, a small amount of noise ($\sigma \ll 0.01$) can be mitigated by the models, but with larger noise ($\sigma \gtrapprox 0.01$), the predictions become highly unreliable. Since the evaluation of more "realistic samples" (e.g., acquired from the production process of a brewery) were not the subject of this work, we could not verify if the artificially generated noise used in this study corresponds to a real process setting. Consequently, we have no information about the magnitude of σ either. However, such knowledge is considered mandatory to assess the practical implications of our findings and will be evaluated in future experiments. This will further facilitate the understanding of uncertainties and their impacts on collected datasets. However, the relative robustness of certain ML models to a small amount of artificial noise indicates that it is possible to transfer classifiers trained in a less noisy environment to a somewhat more noisy environment. Monitoring models using RS combined with various other ML models has already proven to be reasonable for the accurate monitoring of the yeast fermentation process [35].

A conclusive comparison of the considered ML approaches for different datasets revealed that GPC is the best overall ML approach, whereas NN is the worst. The relatively poor performance of NN may be the result of the chosen network architecture for the NAS. With a different architecture, the results could, in principle, differ significantly. However, in regard to artificial noise, we found that the NN can lead to very noise-resilient models in a noise regime where other approaches fail.

6. Conclusions

In this study, we evaluated the potential of RS and predictive ML models for the discrimination of viable and heat-inactivated *S. cerevisiae* cells in different background media and a mixed setting. To this end, limited amounts of in vitro measurement data were used to train a total of six different types of models: RF, GB, GPC, SVM, XGB, and NN. We demonstrate that the viability of yeast in a water medium can be predicted with a balanced accuracy of up to 0.84 using SVM with suitable preprocessing of RS data. Similar results could also be achieved for other media. It was only for the mixed setting—where other yeast strains were also present in the sample—that the best-balanced accuracy reached 0.56

using GPC. From statistical tests, GPC has proven to be the best overall ML approach in a direct comparison with the other approaches.

We also discovered that a model trained exclusively with data from yeast in water performs poorly when predicting yeast in other media than water. Thus, we demonstrated that the background medium has a significant influence on the composition of the spectra. Moreover, these observations clearly show that the robustness of model predictions is closely related to the sample composition used for training. We expect a more accurate and robust prediction when the training of ML models is performed on larger datasets from an experimental environment reflecting "real world" conditions.

In summary, our results demonstrate that RS, in combination with ML, is a promising tool for non-invasive inline monitoring of fermentation processes. We were able to demonstrate a working proof-of-concept for our in vitro scenario. Optionally, RS can be used in combination with already established analytical methods, such as for CO_2, turbidity, or temperature. Furthermore, RS allows measuring sugar consumption and ethanol production, providing an even more detailed analytic view of ongoing fermentation processes. On the other hand, the prediction performances of the presented ML models still need to be improved, which could be achieved with a larger set of Raman spectra or special-purpose models that have been optimized for this particular task. The realization of such models could serve as a possible starting point for further research.

Author Contributions: Conceptualization, S.M.B. and M.B.; methodology, J.W., R.H., S.M.B. and M.B.; software, R.H. and M.B.; validation, J.W. and R.H.; formal analysis, R.H. and M.B; investigation, J.W. and R.H.; resources, J.W., S.M.B., R.H. and M.B.; data curation, R.H.; writing—original draft preparation, C.R., J.W., R.H., S.M.B. and M.B.; writing—review and editing, C.R., J.W., R.H., S.M. and M.B.; visualization, R.H.; supervision, S.M.B. and M.B.; project administration, R.H.; funding acquisition, M.B. All authors have read and agreed to the published version of the manuscript.

Funding: This research was funded in parts by DFG (*Deutsche Forschungsgemeinschaft*) within the priority program SPP 2331 under grant number BO 2538/5-1.

Data Availability Statement: The data presented in this study are available upon request.

Acknowledgments: R.H. and M.B. gratefully acknowledge funding from DFG within the priority program SPP 2331 under grant number BO 2538/5-1. The authors acknowledge Lukas Kriem for support with the Raman measurements.

Conflicts of Interest: The authors declare no conflict of interest.

Abbreviations

The following abbreviations are used in this manuscript:

D. bruxellensis	*Dekkera bruxellensis*
XGB	EXtreme Gradient Boosting classifier
GPC	Gaussian process classifier
GB	Gradient boosting classifier
ML	Machine learning
NAS	Neural architecture search
NN	Neural network
PAT	Process analytical technology
RS	Raman spectroscopy
RF	Random forest classifier
S. cerevisiae	*Saccharomyces cerevisiae*
SVM	Support vector machine classifier
YPD	Yeast extract peptone dextrose

Appendix A. Formal Data-Processing Pipeline

In this appendix section, we formally describe our data-processing pipeline from Section 3. As indicated in Section 3, we omit all measurement units to simplify the notation.

Appendix A.1. Data Processing

We preprocessed the data into a unified form that is suitable for ML applications. For each data point n, five preprocessing steps were used:

1. Interpolate the vectors uniformly with a linear transformation $U(\mathbf{K}^n, \mathbf{I}^n)$ by choosing a constant vector of wave numbers

$$U : \mathbf{K}^n \mapsto \tilde{\mathbf{K}} \tag{A1}$$

with $\tilde{\mathbf{K}} := [K_{\text{min}}, K_{\text{min}} + K_\delta \ldots, K_{\text{min}} + 1014K_\delta]$, such that the corresponding interpolated intensity vector reads

$$U : \mathbf{I}^n \mapsto \mathbf{I}'^n. \tag{A2}$$

Here, $K_{\text{min}} \approx 282.770$ and $K_\delta \approx 1.711$.

2. Rescale the intensity vector to the interval $[0, 1]$ with

$$R_1 : \mathbf{I}'^n \mapsto \mathbf{I}''^n \in [0, 1]^{1015} \tag{A3}$$

by applying

$$R_1(\mathbf{I}'^n_i) := \frac{I'^n_i - \min_m I'^m_i}{\max_m I'^m_i - \min_m I'^m_i} \tag{A4}$$

to each element i.

3. Fix a systematic error in the measurement results with

$$G : \mathbf{I}''^n \mapsto \mathbf{I}'''^n \tag{A5}$$

by applying

$$G(I''^n_i) := \begin{cases} (i - 320)\frac{I''^n_{340} - I''^n_{320}}{20} + I''^n_{320} & \text{if } 320 \leq i \leq 340 \\ I''^n_i & \text{otherwise} \end{cases} \tag{A6}$$

to each element i.

4. Perform a baseline correction

$$B : \mathbf{I}'''^n \mapsto \mathbf{I}''''^n. \tag{A7}$$

based on asymmetrically reweighted penalized least squares smoothing (arPLS) [36] with the smoothness parameter $\lambda := 1 \times 10^5$, termination condition ratio $r := 1 \times 10^{-6}$, and maximum number of iterations $\tau := 10$ after the internal loop is stopped.

5. Perform standardization of the intensity vector

$$R_2 : \mathbf{I}''''^n \mapsto \tilde{\mathbf{I}}^n, \tag{A8}$$

by applying

$$R_2(I''''^n_i) := \frac{I''''^n_i - \mu_i}{\sigma_i} \tag{A9}$$

to each element i, with a mean of

$$\mu_i := \frac{1}{N}\sum_n I''''^n_i \tag{A10}$$

and standard deviation

$$\sigma_i := \sqrt{\frac{1}{N}\sum_n (I''''^n_i - \mu_R)^2}, \tag{A11}$$

respectively.

Summarized, the effective preprocessing transformation

$$R_2 \circ B \circ G \circ R_1 \circ U : (\mathbf{K}^n, \mathbf{I}^n) \mapsto (\tilde{\mathbf{K}}, \tilde{\mathbf{I}}^n) \tag{A12}$$

leads to the data shown in Appendix B.

Appendix A.2. Artificial Noise

We also considered data that have been perturbed by artificially generated noise. For this purpose, we extended the preprocessing transformation, (A12), by an additional step after the first rescaling, (A3), i.e., between steps two and three. In this additional step, we performed a perturbation

$$V(\sigma) : \mathbf{I}'^n \mapsto \mathbf{I}''^n(\sigma) \in \mathbb{R}^{1015} \tag{A13}$$

by applying

$$V(\mathbf{I}''^n_i; \sigma) := I''^n_i + v^n_i(\sigma), \tag{A14}$$

where $v^n_i(\sigma)$ denotes random variables drawn from a normal distribution with the vanishing mean and standard deviation $\sigma > 0$. For the noiseless case $\sigma = 0$, we set the constant value $v^n_i(\sigma = 0) := 0$. To summarize,, the perturbed preprocessing transformation is given by

$$R_2 \circ B \circ G \circ V(\sigma) \circ R_1 \circ U : (\mathbf{K}^n, \mathbf{I}^n) \mapsto (\tilde{\mathbf{K}}, \tilde{\mathbf{I}}^n(\sigma)) \tag{A15}$$

instead of (A12).

Appendix B. Data Visualization

In this appendix section, we visualize the datasets that resulted from our preprocessing method, which is explained in Appendix A. In Figures A1–A3, we show the mean $\mathbb{E}_n \tilde{I}^n_i$ and standard deviation $\mathbb{V}_n \tilde{I}^n_i$ of each preprocessed dataset, divided into data for $y = 1$ (yeast viable) and $y = 0$ (yeast heat-inactivated). As indicated in Section 3, we omit all measurement units. To demonstrate the effects of different values of σ from artificial noise, we additionally plot the expected standard deviation over all wavelengths $\mathbb{E}_i \mathbb{V}_n \tilde{I}^n_i(\sigma)$ in Figure A4, where we also show the corresponding standard deviation $\mathbb{V}_i \mathbb{V}_n \tilde{I}^n_i(\sigma)$. As expected, the signal-to-noise ratio decreases as the perturbation increases.

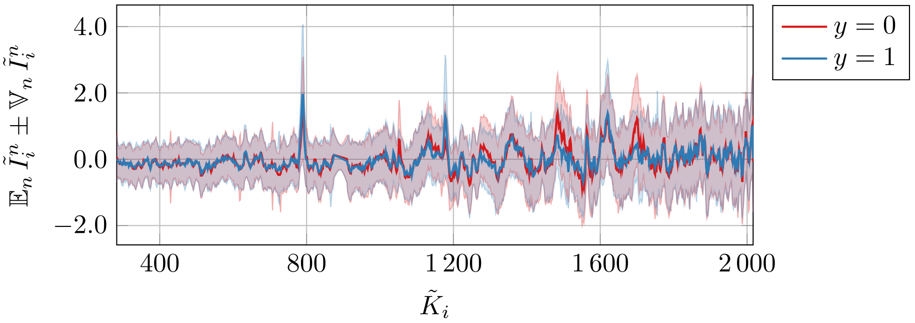

Figure A1. Mean and standard deviation of all datasets from Table 1 after the preprocessing.

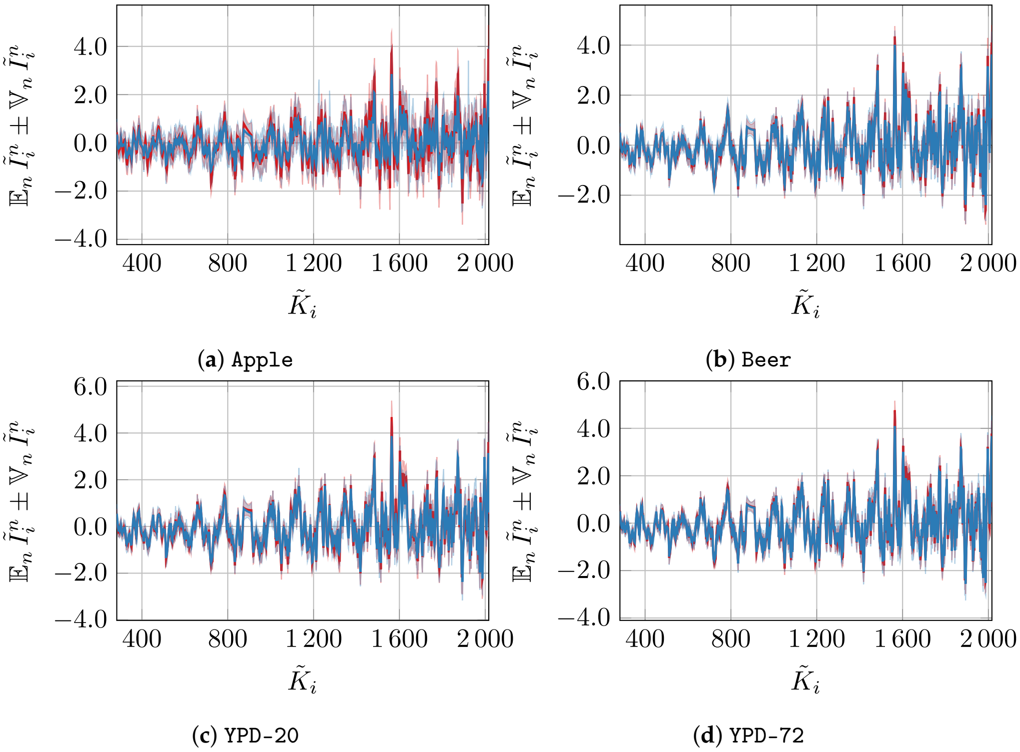

(**a**) `Apple`

(**b**) `Beer`

(**c**) `YPD-20`

(**d**) `YPD-72`

Figure A2. Mean and standard deviation of all datasets from Table 2 in analogy to Figure A1.

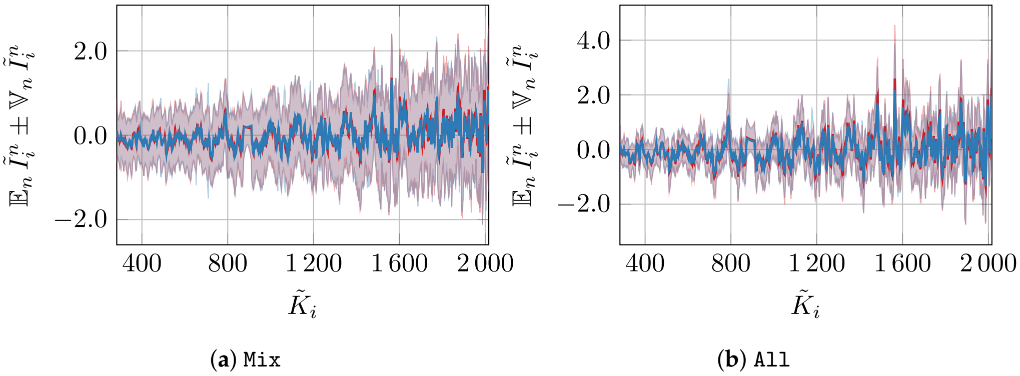

(**a**) `Mix`

(**b**) `All`

Figure A3. Mean and standard deviation of all datasets from Table 3 in analogy to Figure A1.

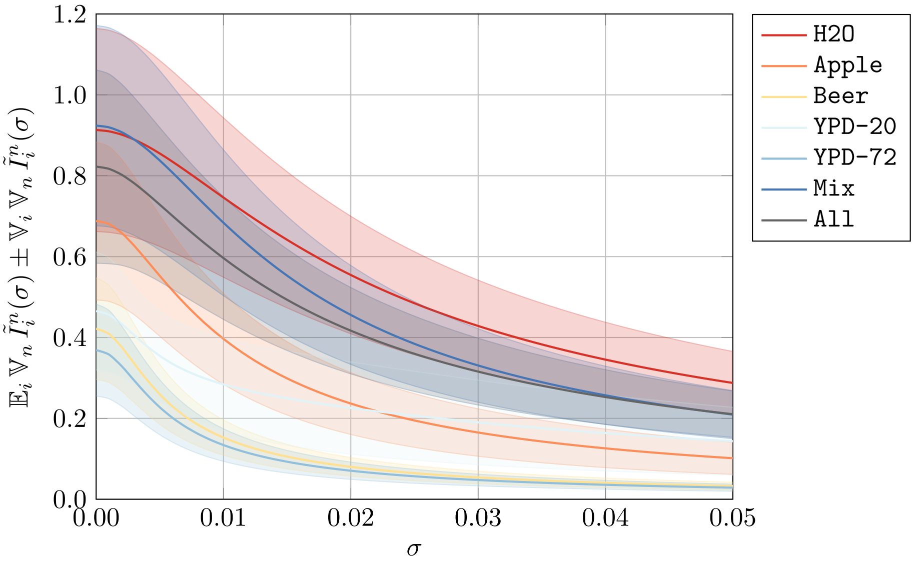

Figure A4. Mean and standard deviation for artificially perturbed data as defined in Section 3.

Appendix C. Machine Learning Model Specifications

In this appendix section, we list the details of the chosen ML approaches from Section 3:

1. RF: We used the implementation `RandomForestClassifier` from scikit-learn [32] with the parameter `n_estimators` = 250.
2. GB: We used the implementation `HistGradientBoostingClassifier` from scikit-learn [32] with the parameter `max_iter` = 250.
3. XGB: We used the implementation `XGBClassifier` from [37].
4. GPC: We used the implementation `GaussianProcessClassifier` from scikit-learn [32] with the parameters `kernel` = 1.0 ∗ `RBF`(1.0) and `n_restarts_optimizer` = 25.
5. SVM: We used the implementation `SVC` from scikit-learn [32] with the parameter `gamma` = `'auto'`.
6. NN: We used PyTorch [38] with Keras [39] and Optuna [40] to realize the neural network. To this end, we utilized NAS to determine the structure of the network. In total, we specified nine NAS parameters that are all defined within the Optuna framework:
   (a) `n_conv_layers` $\in \{0, \dots, 4\}$,
   (b) `filters` $\in \{2, \dots, 16\}$,
   (c) `kernel_size` $\in \{2, \dots, 32\}$,
   (d) `strides` $\in \{2, 4, 6, \dots, 32\}$,
   (e) `n_dense_layers` $\in \{0, \dots, 4\}$,
   (f) `dense_size` $\in \{2, \dots, 32\}$,
   (g) `dropout_active` $\in \{0, 1\}$,
   (h) `dropout_rate` $\in [0, 0.75]$ and
   (i) `learning_rate` $\in [1 \times 10^{-4}, 1 \times 10^{-2}]$.

   Based on these parameters, the neural network was created as follows:

   (a) An input layer `keras.layers.Input` is followed by
   (b) `n_conv_layers` layers `keras.layers.Conv1D` with the following options:
      i. `filters`, `kernel_size`, and `strides`, according to the respective NAS parameter,
      ii. `padding` = `'same'`,
      iii. `kernel_initializer` = `'glorot_uniform'`,
      iv. `activation` = `'relu'`, and
      v. `bias_initializer` = `'zeros'`.

      Each layer is followed by `keras.layers.BatchNormalization`.
   (c) If `n_conv_layers` is non-zero, the convolutional layers are finalized with `keras.layers.GlobalAveragePooling1D`, otherwise, `keras.layers.Flatten` is used.
   (d) Next, `n_dense_layers` layers `keras.layers.Dense` are added with the following options:
      i. `dense_size` according to the respective NAS parameter,
      ii. `activation` = `'relu'`,
      iii. `kernel_initializer` = `'glorot_uniform'`, and
      iv. `bias_initializer` = `'zeros'`.
   (e) If `dropout_active` is one, each dense layer is supplemented by `keras.layers.Dropout(dropout_rate)`.
   (f) Finally, the output layer `keras.layers.Dense` is added with the following options:
      i. `units` = 2,
      ii. `activation` = `'softmax'`,
      iii. `kernel_initializer` = `'glorot_uniform'`, and
      iv. `bias_initializer` = `'zeros'`.

   The neural networks were trained with `keras.optimizers.Adam` with the following options:

(a) `learning_rate` according to the respective NAS parameter and
(b) A validation split of 0.1 on the sparse categorical cross-entropy loss function.

In addition, we made use of the callback functions `keras.callbacks.ReduceLROnPlateau` and `keras.callbacks.EarlyStopping`, respectively, during the training procedure. The neural network test accuracy score averaged over all stratified 10-folds was chosen as the NAS goal function.

For all unspecified parameters, the default values of the respective implementations were used.

References

1. Spencer, J.F.; Spencer, D.M. *Yeasts in Natural and Artificial Habitats*; Springer Science & Business Media: Berlin/Heidelberg, Germany, 1997.
2. Gibson, B.R.; Lawrence, S.J.; Leclaire, J.P.; Powell, C.D.; Smart, K.A. Yeast responses to stresses associated with industrial brewery handling. *FEMS Microbiol. Rev.* **2007**, *31*, 535–569. [CrossRef] [PubMed]
3. Matallana, E.; Aranda, A. Biotechnological impact of stress response on wine yeast. *Lett. Appl. Microbiol.* **2017**, *64*, 103–110. [CrossRef] [PubMed]
4. Baradez, M.O.; Biziato, D.; Hassan, E.; Marshall, D. Application of Raman Spectroscopy and Univariate Modelling As a Process Analytical Technology for Cell Therapy Bioprocessing. *Front. Med.* **2018**, *5*, 47. [CrossRef]
5. Boyd, A.R.; Gunasekera, T.S.; Attfield, P.V.; Simic, K.; Vincent, S.F.; Veal, D.A. A flow-cytometric method for determination of yeast viability and cell number in a brewery. *FEMS Yeast Res.* **2003**, *3*, 11–16. [CrossRef] [PubMed]
6. Pierce, J.; Committee, A. Institute of Brewing: Analysis committee measurement of yeast viability. *J. Inst. Brew.* **1970**, *76*, 442–443. [CrossRef]
7. Boulton, C.; Quain, D. *Brewing Yeast and Fermentation*; Wiley: Hoboken, NJ, USA, 2008.
8. Thomson, K.; Bhat, A.; Carvell, J. Comparison of a new digital imaging technique for yeast cell counting and viability assessments with traditional methods. *J. Inst. Brew.* **2015**, *121*, 231–237. [CrossRef]
9. Luoma, P.; Golabgir, A.; Brandstetter, M.; Kasberger, J.; Herwig, C. Workflow for multi-analyte bioprocess monitoring demonstrated on inline NIR spectroscopy of P. chrysogenum fermentation. *Anal. Bioanal. Chem.* **2016**, *409*, 797–805. [CrossRef]
10. Hirsch, E.; Pataki, H.; Domján, J.; Farkas, A.; Vass, P.; Fehér, C.; Barta, Z.; Nagy, Z.K.; Marosi, G.J.; Csontos, I. Inline noninvasive Raman monitoring and feedback control of glucose concentration during ethanol fermentation. *Biotechnol. Prog.* **2019**, *35*, e2848. [CrossRef]
11. Wieland, K.; Masri, M.; von Poschinger, J.; Brück, T.; Haisch, C. Non-invasive Raman spectroscopy for time-resolved in-line lipidomics. *RSC Adv.* **2021**, *11*, 28565–28572. [CrossRef]
12. Esmonde-White, K.A.; Cuellar, M.; Lewis, I.R. The role of Raman spectroscopy in biopharmaceuticals from development to manufacturing. *Anal. Bioanal. Chem.* **2022**, *414*, 969–991. [CrossRef]
13. Rösch, P.; Harz, M.; Schmitt, M.; Peschke, K.D.; Ronneberger, O.; Burkhardt, H.; Motzkus, H.W.; Lankers, M.; Hofer, S.; Thiele, H.; et al. Chemotaxonomic identification of single bacteria by micro-Raman spectroscopy: Application to clean-room-relevant biological contaminations. *Appl. Environ. Microbiol.* **2005**, *71*, 1626–1637. [CrossRef] [PubMed]
14. Wulf, M.W.H.; Willemse-Erix, D.; Verduin, C.M.; Puppels, G.; van Belkum, A.; Maquelin, K. The use of Raman spectroscopy in the epidemiology of methicillin-resistant Staphylococcus aureus of human- and animal-related clonal lineages. *Clin. Microbiol. Infect.* **2011**, *18*, 147–152. [CrossRef]
15. Meisel, S.; Stöckel, S.; Elschner, M.; Melzer, F.; Rösch, P.; Popp, J. Raman spectroscopy as a potential tool for detection of Brucella spp. in milk. *Appl. Environ. Microbiol.* **2012**, *78*, 5575–5583. [CrossRef] [PubMed]
16. Stöckel, S.; Meisel, S.; Elschner, M.; Rosch, P.; Popp, J. Identification of Bacillus anthracis via Raman spectroscopy and chemometric approaches. *Anal. Chem.* **2012**, *84*, 9873–9880. [CrossRef] [PubMed]
17. Hamasha, K.; Mohaidat, Q.I.; Putnam, R.A.; Woodman, R.C.; Palchaudhuri, S.; Rehse, S.J. Sensitive and specific discrimination of pathogenic and nonpathogenic Escherichia coli using Raman spectroscopy—A comparison of two multivariate analysis techniques. *Biomed. Opt. Express* **2013**, *4*, 481–489. [CrossRef]
18. Zhu, X.; Xu, T.; Lin, Q.; Duan, Y. Technical Development of Raman Spectroscopy: From Instrumental to Advanced Combined Technologies. *Appl. Spectrosc. Rev.* **2014**, *49*, 64–82. [CrossRef]
19. Yaseen, T.; Sun, D.W.; Cheng, J.H. Raman imaging for food quality and safety evaluation: Fundamentals and applications. *Trends Food Sci. Technol.* **2017**, *62*, 177–189. [CrossRef]
20. Lintvedt, T.A.; Andersen, P.V.; Afseth, N.K.; Marquardt, B.; Gidskehaug, L.; Wold, J.P. Feasibility of In-Line Raman Spectroscopy for Quality Assessment in Food Industry: How Fast Can We Go? *Appl. Spectrosc.* **2022**, *76*, 559–568. [CrossRef]
21. Khan, H.H.; McCarthy, U.; Esmonde-White, K.; Casey, I.; O'Shea, N. Potential of Raman spectroscopy for in-line measurement of raw milk composition. *Food Control* **2023**, *152*, 109862. [CrossRef]
22. Woolfit, M.; Rozpedowska, E.; Piskur, J.; Wolfe, K.H. Genome survey sequencing of the wine spoilage yeast Dekkera (Brettanomyces) bruxellensis. *Eukaryot Cell* **2007**, *6*, 721–733. [CrossRef]
23. Bishop, C.M. *Pattern Recognition and Machine Learning*; Springer: Berlin/Heidelberg, Germany, 2006.

24. James, G.; Witten, D.; Hastie, T.; Tibshirani, R.; Taylor, J. *An Introduction to Statistical Learning: With Applications in Python*; Springer Texts in Statistics; Springer International Publishing: Berlin/Heidelberg, Germany, 2023.
25. Breiman, L. Random Forests. *Mach. Learn.* **2001**, *45*, 5–32. .:1010933404324. [CrossRef]
26. Friedman, J.H. Greedy function approximation: A gradient boosting machine. *Ann. Stat.* **2001**, *29*, 1189–1232. [CrossRef]
27. Chen, T.; Guestrin, C. XGBoost. In Proceedings of the 22nd ACM SIGKDD International Conference on Knowledge Discovery and Data Mining, San Francisco, CA, USA, 13–17 August 2016. [CrossRef]
28. Rasmussen, C.E.; Williams, C.K.I. *Gaussian Processes for Machine Learning*; MIT Press: Cambridge, MA, USA, 2005.
29. Cortes, C.; Vapnik, V. Support-vector networks. *Mach. Learn.* **1995**, *20*, 273–297. [CrossRef]
30. Cervantes, J.; Garcia-Lamont, F.; Rodríguez-Mazahua, L.; Lopez, A. A comprehensive survey on support vector machine classification: Applications, challenges and trends. *Neurocomputing* **2020**, *408*, 189–215. [CrossRef]
31. Schmidhuber, J. Deep learning in neural networks: An overview. *Neural Netw.* **2015**, *61*, 85–117. [CrossRef]
32. Pedregosa, F.; Varoquaux, G.; Gramfort, A.; Michel, V.; Thirion, B.; Grisel, O.; Blondel, M.; Prettenhofer, P.; Weiss, R.; Dubourg, V.; et al. Scikit-learn: Machine Learning in Python. *J. Mach. Learn. Res.* **2011**, *12*, 2825–2830.
33. Dietterich, T.G. Approximate Statistical Tests for Comparing Supervised Classification Learning Algorithms. *Neural Comput.* **1998**, *10*, 1895–1923. [CrossRef] [PubMed]
34. Welch, B.L. The generalization of Student's Problem when several different population variances are involved. *Biometrika* **1947**, *34*, 28–35. [CrossRef]
35. Jiang, H.; Xu, W.; Ding, Y.; Chen, Q. Quantitative analysis of yeast fermentation process using Raman spectroscopy: Comparison of CARS and VCPA for variable selection. *Spectrochim. Acta Part A Mol. Biomol. Spectrosc.* **2020**, *228*, 117781. [CrossRef]
36. Baek, S.J.; Park, A.; Ahn, Y.J.; Choo, J. Baseline correction using asymmetrically reweighted penalized least squares smoothing. *Analyst* **2015**, *140*, 250–257. [CrossRef]
37. dmlc GitHub. XGBoost Python Package. 2022. Available online: https://github.com/dmlc/xgboost/tree/master/python-package (accessed on 6 December 2022).
38. Paszke, A.; Gross, S.; Massa, F.; Lerer, A.; Bradbury, J.; Chanan, G.; Killeen, T.; Lin, Z.; Gimelshein, N.; Antiga, L.; et al. PyTorch: An Imperative Style, High-Performance Deep Learning Library. In *Advances in Neural Information Processing Systems 32*; Wallach, H., Larochelle, H., Beygelzimer, A., d' Alché-Buc, F., Fox, E., Garnett, R., Eds.; Curran Associates, Inc.: Red Hook, NY, USA, 2019; pp. 8024–8035.
39. Chollet, F. Keras. 2015. Available online: https://keras.io (accessed on 6 December 2022).
40. Akiba, T.; Sano, S.; Yanase, T.; Ohta, T.; Koyama, M. Optuna: A Next-generation Hyperparameter Optimization Framework. In Proceedings of the 25rd ACM SIGKDD International Conference on Knowledge Discovery and Data Mining, Anchorage, AK, USA, 4–8 August 2019.

Disclaimer/Publisher's Note: The statements, opinions and data contained in all publications are solely those of the individual author(s) and contributor(s) and not of MDPI and/or the editor(s). MDPI and/or the editor(s) disclaim responsibility for any injury to people or property resulting from any ideas, methods, instructions or products referred to in the content.